SU(2) hyper-clocks: Quantum engineering of spinor interferences for time and frequency metrology

Thomas Zanon-Willette

SU(2) hyper-clocks: Quantum engineering of spinor interferences for time and frequency metrology

T. Zanon-Willette,[1,2,3,*] D. Wilkowski,[2,3,4] R. Lefevre,[5] A. V. Taichenachev,[6,7] and V. I. Yudin[6,7,8]

[1]*Observatoire de Paris, Sorbonne Université, Université PSL, CNRS, LERMA, F-75005 Paris, France*
[2]*MajuLab, International Research Laboratory IRL 3654, Université Côte d'Azur, Sorbonne Université, National University of Singapore, Nanyang Technological University, Singapore*
[3]*Centre for Quantum Technologies, National University of Singapore, 117543 Singapore*
[4]*School of Physical and Mathematical Sciences, Nanyang Technological University, 637371 Singapore*
[5]*Department of Physics, Royal Holloway, University of London, Royal Holloway Egham Hill, Egham TW20 0EX, United Kingdom*
[6]*Novosibirsk State University, ulica Pirogova 2, 630090 Novosibirsk, Russia*
[7]*Institute of Laser Physics, Siberian Branch, Russian Academy of Sciences, Prospekt Akademika Lavrent'eva 15B, 630090 Novosibirsk, Russia*
[8]*Novosibirsk State Technical University, Prospekt Karla Marksa 20, 630073 Novosibirsk, Russia*

(Received 18 January 2022; accepted 19 April 2022; published 13 May 2022)

In 1949, Ramsey's method [Phys. Rev. **76**, 996 (1949)] of separated oscillating fields was elaborated boosting over many decades metrological performances of atomic clocks and becoming the standard technique for very high-precision spectroscopic measurements. A generalization of this interferometric method is presented replacing the two single coherent excitations by arbitrary composite laser pulses. The rotation of the state vector of a two-level system under the effect of a single pulse is described using the Pauli matrices basis of the SU(2) group. It is then generalized to multiple excitation pulses by a recursive Euler-Rodrigues-Gibbs algorithm describing a composition of rotations with different rotation axes. A general analytical formula for the phase shift associated with the clock's interferometric signal is derived. As illustrations, hyper-clocks based on three-pulse and five-pulse interrogation protocols are studied and shown to exhibit nonlinear cubic and quintic sensitivities to residual probe-induced light shifts. The presented formalism is well suited to optimize composite phase shifts produced by tailored quantum algorithms in order to design a new generation of optical frequency standards and robust engineering control of atomic interferences in atomic, molecular, and optical physics with cold matter and antimatter.

DOI: 10.1103/PhysRevResearch.4.023117

I. INTRODUCTION

The method of separated oscillating fields was introduced by Ramsey in 1949 to improve frequency resolution of spectroscopic measurements and collect information about the internal structure of atoms and molecules [1–3]. Today, understanding how to improve the robustness of spectroscopy with coherent radiation by reducing or eliminating laser probe-induced systematics still remains a central goal in the broad and important field of robust atomic sensors from stringent tests of fundamental physics to quantum metrology with optical clocks and matter-wave interferometry [4].

Ramsey derived in 1950 the first original quantum-mechanical description of a spin-1/2 interferometric resonance with two separated coherent pulses by using a Schrödinger wave-function description [2] later extending the analysis to phase jumps, pulse shapes, and amplitudes [5,6]. Ramsey's method became the standard technique in atomic physics based on microwave and laser spectroscopy and in quantum metrology with atomic beams [7] and cold atomic fountains [8] to measure transition frequencies between particle states with very high precision [9]. After 70 yr, Ramsey interferometry is still a powerful tool to investigate matter-light interaction with a few particles, such as in modern cavity QED experiments on Schrödinger's cats with Rydberg's atoms [10–12], in quantum information with trapped ions [13] or with superconducting qubits [14].

Nevertheless, the architecture of the two-pulse Ramsey interferometer as shown in Fig. 1 has remained untouched until 2010 when an improvement for clock spectroscopy was proposed [15,16] and experimentally applied to a single trapped ion [17]. A Ramsey sequence of two coherent laser pulses is used with a precompensation of the estimated light shift including a third intermediate pulse which is inserted to act, such as a spin-echo compensation of field amplitude error [15,16,18,19]. After the experimental success of the hyper-Ramsey protocol to drastically reduce by four orders of magnitude the residual light shift on the single-ion $^{171}Yb^{+}$ octupole clock transition [20], more robust generalized hyper-Ramsey three-pulse protocols have been discovered against laser pulse-induced frequency shifts [21] including decoherence effect [22–24]. Naturally, the question arises if there is

*thomas.zanon@sorbonne-universite.fr

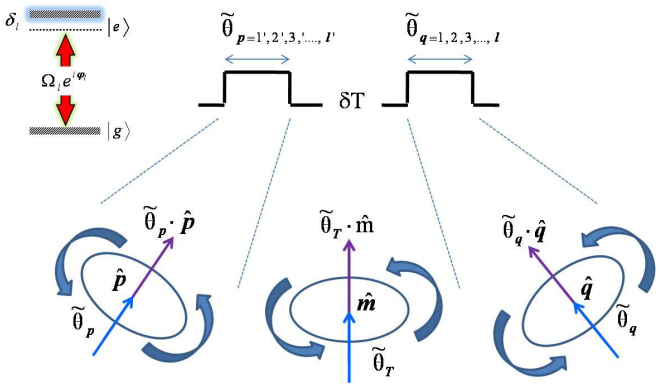

FIG. 1. Generalized Ramsey's method of separated oscillating fields with angle-axis representation. Single pulses (or sets of composite pulses) around a single Ramsey free evolution phase as δT are introduced by effective pulse areas $\widetilde{\theta}_p$ and $\widetilde{\theta}_q$ where $p \equiv 1'$–$3' \ldots$, $q \equiv 1$–$3 \cdots$ with arbitrary rotation axis orientations $\widehat{n}_p$ and $\widehat{n}_q$ around the $\widehat{m}$ axis. Single or composite laser pulse parameters are including laser phase φ_p, φ_q, field excitation Ω_p, Ω_q, pulse duration τ_p, τ_q, and a frequency detuning $\delta_p = \delta \mp \Delta_p$, $\delta_q = \delta \mp \Delta_q$ including the uncompensated part of the light-shift Δ_p, Δ_q during pulses [15]. Any residual light shift is inducing a weak distortion of the angle-axis orientation relative to the intermediate free evolution zone.

a way to extend interrogation protocols to any sets of arbitrary composite pulses around a single free evolution time in a symmetrical fashion. The first positive answer including composite laser pulses was provided through a Cayley-Klein parametrization of rotation spinors [25]. An extended model based on multiple hyper-Ramsey-Bordé building blocks with two-level operators and quantization of motion has been recently developed where arbitrary composite optical pulses are used not only to shield quantum clock interferences against residual light shift, but also to protect atomic matter waves against laser probe-induced frequency shifts at ultracold temperature [4]. A complementary approach to Ref. [4], extending [25], would be strongly helpful in designing new sequences of laser pulses to compensate for their systematic errors in pulse detuning, relative phase, and/or pulse area through various robust quantum control techniques [26–30].

The purpose of this paper is to present an alternative formalism to Refs [4,16,25] allowing a convenient derivation of generalized hyper-Ramsey clock interferences and atomic phase shifts with arbitrary composite pulses and axis orientation. Exponentials of Pauli matrices [31] are used to decompose a complex transition amplitude following an initial suggestion by Rabi *et al.* [32]. Multiple interactions between the two-level system (or qubit) and laser pulses will be treated as a composition of spinor rotations on a Bloch sphere. Furthermore, a recursive algorithm based on the Euler-Rodrigues-Gibbs geometrical transformation for dual axis rotation composition [33–37] is extended to qubit rotation allowing a systematic exploration and optimization of more elaborated interrogation protocols with multiple laser pulses.

The recursive algorithm has been inspired by composite pulses developed originally in NMR [38–40] where composition of two rotations with quaternion computation rules [41,42] have already been applied to facilitate geometrical analysis and the role of symmetry in the design of composite pulse action on nuclear spin ensembles [43,44]. More recently, the Schrödinger equation has been reexplored within a quaternionic representation of a Pauli spinor of an electron [45], and a quaternionic derivation of the Ramsey transition probability has been presented [46] providing an alternative way to compute composite rotations on the Bloch sphere.

The paper is organized as follows: in Sec. II, we introduce a vectorial representation of spinor matrix components associated with complex transition amplitudes. Then, a compact expression of the composite phase shift associated with quantum interferences with multipulses is given in Sec. III. From a quantum engineering perspective, the best tailoring approach of atomic interferences is tracked to produce by pulse engineering methods, such as quantum control [47,48], an optimization of some targeted performances, i.e., frequency shift and signal amplitude of optical clocks to make more robust to important variations of relevant experimental parameters. Finally, exact expressions of atomic phase shifts are derived. Here, we are mainly focusing on specific laser pulse protocols on three-pulse and five-pulse schemes related to the design of hyper-Ramsey composite phase shifts for ultrarobust optical clocks [16,25,49]. Such hyper-clocks produce various highly nonlinear, flexible, and robust compensation of the residual light shift with a different sensitivity to laser probe intensity fluctuation [50]. SU(2) hyper-clocks are a class of optical qubit clocks based on composite laser pulse protocols aimed at reducing laser probe-induced frequency shifts by several orders of magnitude improving the accuracy of optical clocks.

II. VECTORIAL REPRESENTATION OF GENERALIZED HYPER-RAMSEY SPINOR COMPONENTS

A. Pauli-spin decomposition

The model is based on a SU(2) Pauli-spin decomposition of generalized hyper-Ramsey resonances and phase shifts. Exact expressions are derived for spinor components of a unitary interaction matrix describing coherent interaction between a qubit and laser excitation pulses. The time-dependent atomic wave-function $\Psi(t) = C_g(t)|g\rangle + C_e(t)|e\rangle$ is interacting with two pulses labeled by p and q and separated by a single free evolution time T as reported in Fig. 1, inducing a qubit rotation composition as [32]

$$\begin{aligned}\Psi(t) &= e^{i\widetilde{\theta}_q(\widehat{n}_q\cdot\vec{\sigma})} e^{i\theta_m(\widehat{m}\cdot\vec{\sigma})} e^{i\widetilde{\theta}_p(\widehat{n}_p\cdot\vec{\sigma})}\Psi(0)\\ &= {}^{q}_{p}C\Psi(0).\end{aligned} \tag{1}$$

The Pauli vector is defined by $\vec{\sigma} = \sigma_x\widehat{x} + \sigma_y\widehat{y} + \sigma_z\widehat{z}$. Rotation axis definitions corresponding to Eq. (1) are introduced by $\widehat{n}_p = \vec{n}_p/\|\vec{n}_p\|$, $\widehat{m} = \vec{m}/\|\vec{m}\|$, and $\widehat{n}_q = \vec{n}_q/\|\vec{n}_q\|$. Rotation angles and angular velocities are defined by $\widetilde{\theta}_p = \|\vec{n}_p\|\tau/2$, $\widetilde{\theta}_m = \|\vec{m}\|T/2$, and $\widetilde{\theta}_q = \|\vec{n}_q\|\tau/2$ with Cartesian unit vector coordinates $\vec{n}_p = (n_{p_x}, n_{p_y}, n_{p_z})$, $\vec{m} = (m_x, m_y, m_z)$, and $\vec{n}_q = (n_{q_x}, n_{q_y}, n_{q_z})$ [39,40]. The 2×2 matrix components ${}^{q}_{p}C_{u,u'}$ are written as

$${}^{q}_{p}C = \begin{pmatrix} {}^{q}_{p}C_{gg} & {}^{q}_{p}C_{ge} \\ {}^{q}_{p}C_{eg} & {}^{q}_{p}C_{ee} \end{pmatrix}, \tag{2}$$

where $u, u' = g, e$. Relations between the components of the unitary interaction matrix correspond to the SU(2) group, namely, ${}^q_pC_{gg} = \{{}^q_pC_{ee}\}^*$, ${}^q_pC_{ge} = -\{{}^q_pC_{eg}\}^*$, and $|{}^q_pC_{gg}|^2 + |{}^q_pC_{ge}|^2 = 1$.

Any general unitary operator corresponding to a rotation of a qubit around a rotation axis $\widehat{n}_l$ with a rotation angle $\widetilde{\vartheta}_l$ ($l = p, q$) is evaluated by the exponential Pauli-spin decomposition [31,51],

$$e^{i\widetilde{\vartheta}_l(\widehat{n}_l\cdot\vec{\sigma})} = \sigma_0 \cos\,\widetilde{\vartheta}_l + i(\widehat{n}_l\cdot\vec{\sigma})\sin\,\widetilde{\vartheta}_l, \tag{3}$$

with the identity Pauli matrix σ_0 and satisfying the vectorial identity relation [51],

$$(\widehat{n}_p\cdot\vec{\sigma})\cdot(\widehat{n}_q\cdot\vec{\sigma}) = (\widehat{n}_p\cdot\widehat{n}_q)\sigma_0 + i(\widehat{n}_p\times\widehat{n}_q)\cdot\vec{\sigma}. \tag{4}$$

The computational procedure calculates the transition probability for a reorientation of the qubit state u into a state u'. It is simply given by ${}^q_pP_{uu'} = |{}^q_pC_{uu'}|^2$ where each spinor component of the unitary matrix is expressed as [19,21,24,25]

$${}^q_pC_{uu'} = {}^q_p\widetilde{C}^+_{uu'}e^{i{}^q_p\widetilde{\Phi}^+_{uu'}}e^{i\widetilde{\theta}_m} + {}^q_p\widetilde{C}^-_{uu'}e^{i{}^q_p\widetilde{\Phi}^-_{uu'}}e^{-i\widetilde{\theta}_m}. \tag{5}$$

The phase-shift difference between components ${}^q_p\widetilde{C}^\pm_{uu'}$ is introduced as

$${}^q_p\widetilde{\Phi}_{uu'} = {}^q_p\widetilde{\Phi}^+_{uu'} - {}^q_p\widetilde{\Phi}^-_{uu'}. \tag{6}$$

Envelopes ${}^q_p\widetilde{C}^\pm_{uu'}$ are themselves expressed with a complex modulus as [52,53]

$${}^q_p\widetilde{C}^\pm_{uu'} = \tfrac{1}{2}(\cos\,\widetilde{\theta}_p\cos\,\widetilde{\theta}_q)\,{}^q_pC^\pm\sqrt{1+\tan^2\left({}^q_p\widetilde{\Phi}^\pm_{uu'}\right)}, \tag{7}$$

and

$${}^q_pC^\pm = \sigma_0 \pm \widehat{m}\cdot\vec{\sigma} \pm \left[{}^q_p\widehat{N}_-\times\widehat{m}\right]\cdot\vec{\sigma} - {}^q_p\widehat{N}^{\widehat{m}}_\bullet. \tag{8}$$

Atomic phase-shifts $\widetilde{\Phi}_{uu'}(\pm)$ associated with ${}^q_p\widetilde{C}^\pm_{uu'}$ are also evaluated with Pauli-spin matrices and are expressed with a complex argument [52,53],

$$\tan{}^q_p\widetilde{\Phi}^\pm_{uu'} \equiv \frac{{}^q_p\widehat{N}_+\cdot[\vec{\sigma}\pm\widehat{m}\sigma_0] + {}^q_p\widehat{N}_\times\cdot[\vec{\sigma}\mp\widehat{m}\sigma_0]}{\sigma_0\pm\widehat{m}\cdot\vec{\sigma}\pm\left[{}^q_p\widehat{N}_-\times\widehat{m}\right]\cdot\vec{\sigma} - {}^q_p\widehat{N}^{\widehat{m}}_\bullet}, \tag{9}$$

where,

$$\begin{aligned}
{}^q_p\widehat{N}_+ &\equiv \widehat{n}_p\tan\,\widetilde{\theta}_p + \widehat{n}_q\tan\,\widetilde{\theta}_q,\\
{}^q_p\widehat{N}_- &\equiv \widehat{n}_p\tan\,\widetilde{\theta}_p - \widehat{n}_q\tan\,\widetilde{\theta}_q,\\
{}^q_p\widehat{N}_\times &\equiv \widehat{n}_p\tan\,\widetilde{\theta}_p\times\widehat{n}_q\tan\,\widetilde{\theta}_q,\\
{}^q_p\widehat{N}^{\widehat{m}}_\bullet &\equiv (\widehat{n}_p\cdot\widehat{n}_q)_{\widehat{m},\vec{\sigma}}\tan\,\widetilde{\theta}_p\tan\,\widetilde{\theta}_q,
\end{aligned} \tag{10}$$

with a reduced variable,

$$\begin{aligned}
(\widehat{n}_p\cdot\widehat{n}_q)_{\widehat{m},\vec{\sigma}} &= (\sigma_0\mp\widehat{m}\cdot\vec{\sigma})(\widehat{n}_p\cdot\widehat{n}_q)\\
&\pm[(\widehat{m}\cdot\widehat{n}_p)\widehat{n}_q + (\widehat{m}\cdot\widehat{n}_q)\widehat{n}_p]\cdot\vec{\sigma}.
\end{aligned} \tag{11}$$

Frequency shifts of atomic interferences produced by the laser probe excitation scheme are described by Eq. (9) where the influence of the light shift is to change simultaneously the rotation axis orientation and the effective Rabi frequency as shown in Fig. 1. This equation contains a dot-product (scalar) term as $\widehat{N}_\bullet$ and a cross-product (vectorial) term as $\widehat{N}_\times$ that are effectively related to a composition rule of two unit quaternions [39,41,42] and to the Euler-Rodrigues-Gibbs (ERG) formula for three-dimensional rotation composition [33–35,37]. Pauli-spin matrices $\sigma_{x,y,z}$ as well as the identity matrix σ_0 are used as Hilbert-space pointers to individually address each ${}^q_p\widetilde{\Phi}^\pm_{uu'}$ component associated with diagonal and off-diagonal elements of the spinor matrix [54]. All ${}^q_pC_{uu'}$ components of a rotated qubit by Ramsey spectroscopy with composite pulses can be analytically derived using the Pauli-spin model presented above.

B. ERG transformation rules and recursive algorithm

Turning to a generalized hyper-Ramsey resonance with an arbitrary number of composite pulses, left and right single Pauli-spin qubits from Fig. 1 should be now replaced by composite qubits as follows:

$$\begin{aligned}
e^{i\widetilde{\theta}_p(\widehat{n}_p\cdot\vec{\sigma})} &\equiv \prod_{l=1'}^{\overrightarrow{p}} e^{i\widetilde{\theta}_l(\widehat{n}_l\cdot\vec{\sigma})},\\
e^{i\widetilde{\theta}_q(\widehat{n}_q\cdot\vec{\sigma})} &\equiv \prod_{l=1}^{\overleftarrow{q}} e^{i\widetilde{\theta}_l(\widehat{n}_l\cdot\vec{\sigma})},
\end{aligned} \tag{12}$$

where each arrow indicates the direction to develop the multi-pulse product with growing indices.

In order to track analytically the resulting phase shift associated with composite interferences, a recursive algorithm is presented based on iteration of the ERG transformation applied to composite pulses from the left and right sides of the two-pulse interferometer. The ERG transformation rules, acting on unit vector coordinates, for a given set of $l \in \{p, q\}$ ($-$ for p and $+$ for q) composite pulses are given by

$$\begin{aligned}
\cos\,\widetilde{\theta}_l &\mapsto \cos\,\widetilde{\theta}_l\cos\,\widetilde{\theta}_{l+1}\left[1 - {}^{l+1}_l\widehat{N}^0_\bullet\right],\\
\widehat{n}_l\tan\,\widetilde{\theta}_l &\mapsto \frac{{}^{l+1}_l\widehat{N}_+ \pm {}^{l+1}_l\widehat{N}_\times}{1 - {}^{l+1}_l\widehat{N}^0_\bullet},
\end{aligned} \tag{13}$$

with ${}^{l+1}_l\widehat{N}^0_\bullet \equiv \widehat{n}_l\cdot\widehat{n}_{l+1}\tan\,\widetilde{\theta}_l\tan\,\widetilde{\theta}_{l+1}$.

These rules applied on ${}^q_pC_{uu'}$ components, used as a quantum-processing algorithm, are iterated $p-1$ and $q-1$ times when running with an ensemble of $\{p, q\}$ pulses (see the Appendix for an example). A different recursive algorithm has been developed in Ref. [4] related to a Möbius transformation in conformal mapping [55], for instance, see the reference note in Ref. [56]. A complete geometrical representation of the qubit dynamics is achieved through Feynman-Vernon-Hellwarth coordinates to visualize composite rotations on a Bloch sphere [57]. A straightforward extension of generalized hyper-Ramsey resonances and phase shifts to a higher quantum J spin made of composite qubits with equally energy spaced levels (hyper-qudit clock) is provided by application of the Majorana formula [58–60] or by using a polynomial matrix expansion of spin rotation [61].

III. COMPOSITE PHASE-SHIFT OPTIMIZATION

A. Analytical formula

The Pauli-spin model is now tested in cases when composite pulses are used in Ramsey interferometry. As a demonstration, a few composite phase shifts are derived following our recursive algorithm. The quantization axis is

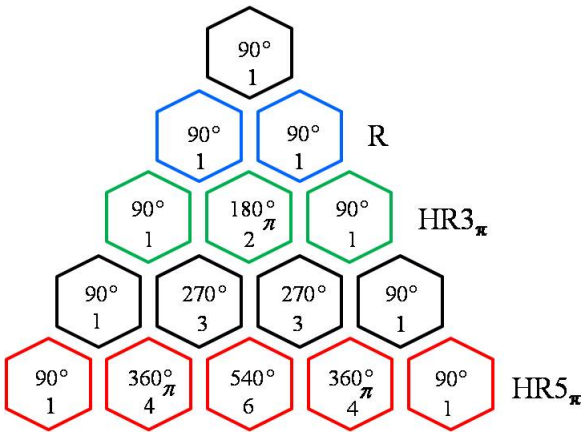

FIG. 2. Hyper-clock protocol classification following Pascal's triangle for binomial coefficient representation. Appropriate laser phase jumps of π are inserted as subscripts within specific laser pulses. Pulse areas are here indicated in integer units of a 90° reference pulse following the time length of each single pulse. The qubit free rotation denoted δT is placed either between the first two pulses or between the last two pulses of $\mathrm{HR3}_\pi$ and $\mathrm{HR5}_\pi$ protocols.

oriented along the z axis as $\widehat{m} = (0, 0, 1)$ for laser pulsed qubit spectroscopy. Normalized unitary rotation axis parameters can be introduced as $\widehat{n}_{l_x} \equiv \frac{\Omega_l}{\omega_l} \cos\varphi_l, \widehat{n}_{l_y} \equiv \frac{\Omega_l}{\omega_l} \sin\varphi_l$, and $\widehat{n}_{l_z} \equiv \frac{\delta_l}{\omega_l}$ ($l \in \{p, q\}$), respectively, related to complex Rabi field frequency on the x, y plane and frequency detuning along the z axis [62]. We, therefore, define the effective Rabi field as $\omega_l = \sqrt{\delta_l^2 + \Omega_l^2}$.

In selected interrogation schemes reported in Fig. 2, dispersive error signals of spinor interferences are produced by subtracting two recorded transition probabilities ${}^q_pP_{gg}$ with additional laser phase-steps $\pm\varphi_l$ opposite in sign and applied on required pulses to produce dispersive curves or interferences [5,21],

$$\Delta E = {}^q_pP_{gg}(+\varphi_l) - {}^q_pP_{gg}(-\varphi_l). \tag{14}$$

Whereas addressing the ${}^q_pC_{gg}$ matrix element with Pauli matrices, the atomic phase-shift expression for a generalized hyper-Ramsey interference with $\{p, q\}$ composite pulses, can always be decomposed into two contributions,

$$\begin{aligned} {}^q_p\widetilde{\Phi}^+_{gg} &= \arctan\left[\frac{()^p_z + ()^q_z}{1 - ()^p_z()^q_z}\right], \\ {}^q_p\widetilde{\Phi}^-_{gg} &= \arctan\left[\frac{()^p_y()^q_x - ()^p_x()^q_y}{()^p_x()^q_x + ()^p_y()^q_y}\right]. \end{aligned} \tag{15}$$

Few elements $()^{p,q}_{x,y,z}$ will be given later. Note that ${}^q_p\widetilde{\Phi}^\pm_{gg}$ can be recast into a single canonical expression as [52]

$${}^q_p\widetilde{\Phi}^+_{gg} \mp {}^q_p\widetilde{\Phi}^-_{gg} = \arctan\left[\frac{\tan{}^q_p\widetilde{\Phi}^+_{gg} \mp \tan{}^q_p\widetilde{\Phi}^-_{gg}}{1 \pm \tan{}^q_p\widetilde{\Phi}^+_{gg}\tan{}^q_p\widetilde{\Phi}^-_{gg}}\right]. \tag{16}$$

Various interrogation protocols are now investigated. Two-pulse, three-pulse, and five-pulse protocols are shown in the diagram of Fig. 2; they can be identified by the rotation angle of each pulse, expressed in terms of an integer multiple of 90°.

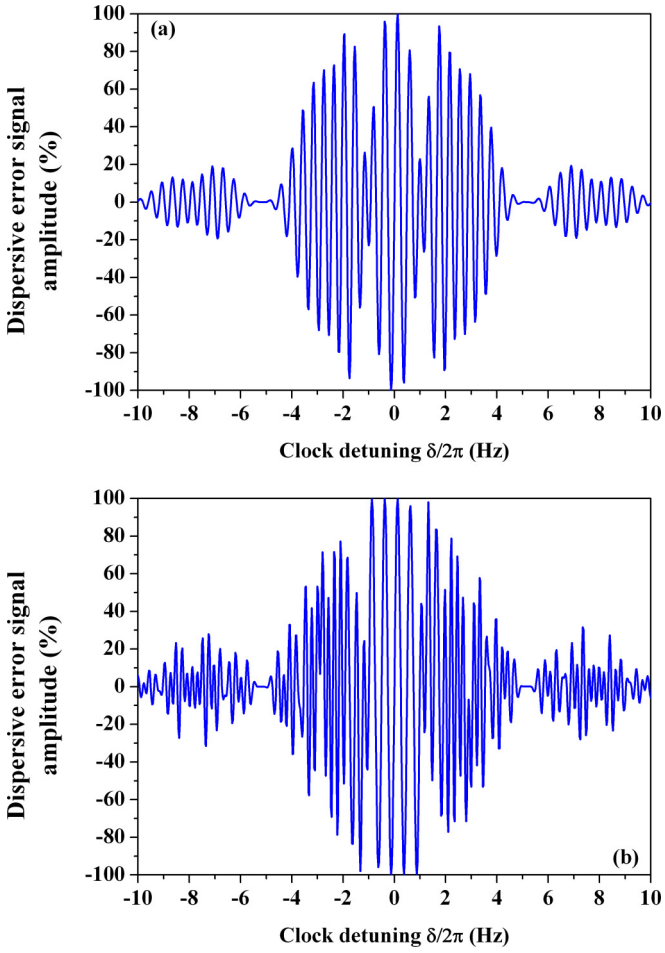

FIG. 3. Two dispersive error signals, calculated from Eq. (14), are plotted versus the clock frequency detuning. (a) $\mathrm{HR3}_\pi$ protocol as $90^\circ_{\pm\pi/2} \dashv \delta\mathrm{T} \vdash 180^\circ_\pi 90^\circ$, (b) $\mathrm{HR5}_\pi$ protocol as $90^\circ_{\pm\pi/2} \dashv \delta\mathrm{T} \vdash 360^\circ_\pi 540^\circ 360^\circ_\pi 90^\circ$. The reference Rabi frequency for all pulses is $\Omega = \pi/2\tau$ ($\Omega\tau \equiv 90^\circ$ area in degrees) where the pulse duration reference is $\tau = 3/16$ s, and the free evolution time is $T = 2$ s.

Using this approach, pulses are classified as Ramsey [1:1] (R, blue), hyper-Ramsey [1:2:1] ($\mathrm{HR3}_\pi$, green) and high-order hyper-Ramsey [1:4:6:4:1] ($\mathrm{HR5}_\pi$, red) protocols following Pascal's triangle for binomial coefficient representation. They can be symmetrically read from left to right or from right to left in the diagram of Fig. 2. This classification is used to identify pulse protocols which make the optical clock sensitive only at high-order levels to the probe laser frequency shifts where the degree of sensitivity scales with the number of pulses. This is also remnant to the Taylor expansion of some leading coefficients of pulse parameters from the theoretical analysis of Refs. [16,23]. The free rotation of the qubit denoted δT has to be positioned between the first two pulses (or the last two pulses) of each configuration. If not, other protocols are generated with a different interferometric line shape and sensitivity to the residual light shift (see, for example, two additional examples of spinor interferences with four pulses shown in Fig. 6 from the Appendix).

The two-pulse R protocol ($p = 1', q = 1$) was proposed in 1949 [1]. The hyper-Ramsey interrogation scheme ($p = 2', q = 1$ or $p = 1', q = 2$) originally presented in 2010, de-

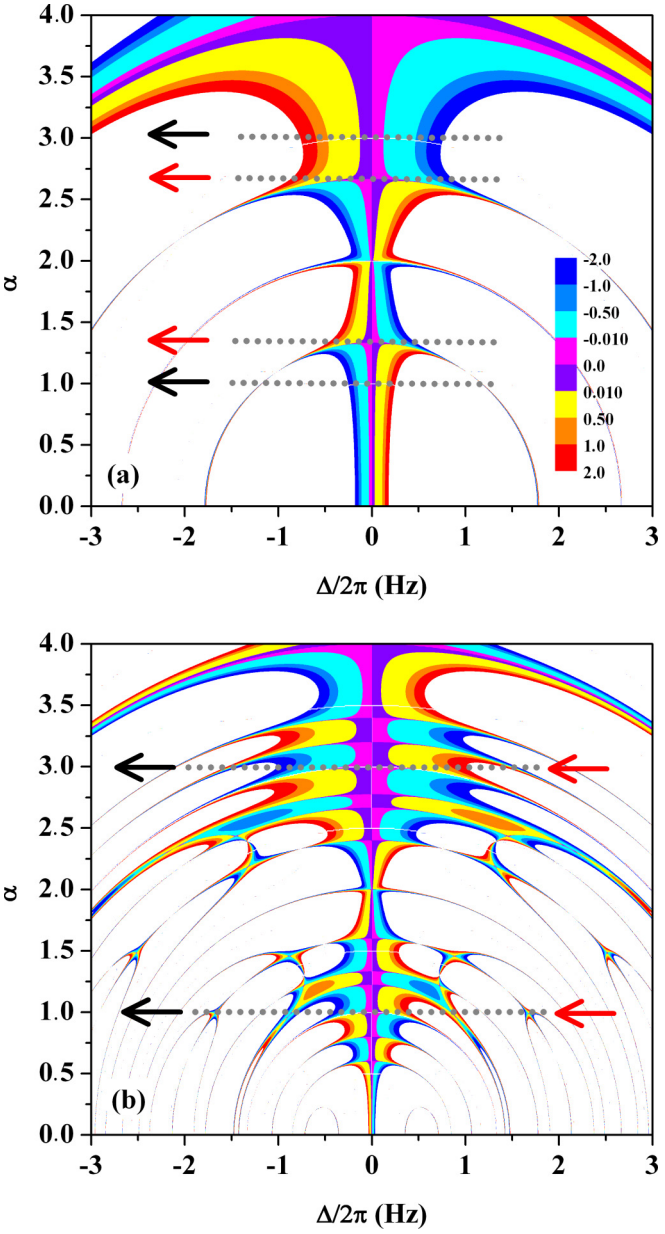

FIG. 4. two-dimensional diagrams of the hyper-Ramsey clock frequency shift (a) ${}^{2}_{1'}\widetilde{\Phi}_{gg}/(2\pi T)$ and (b) ${}^{4}_{1'}\widetilde{\Phi}_{gg}/(2\pi T)$ versus uncompensated part of a residual light-shift $\Delta/2\pi$ along the horizontal axis and pulse area $\Omega\tau$ along the vertical axis (see also Ref. [21]). The only fixed parameter is the free evolution time as $T = 2$ s. Amplitude of the clock frequency shift is indicated by a color graded scale from -2 to 2 mHz on the right side. White regions correspond to values out of range. The reference pulse is $\Omega\tau = \alpha \times \pi/2$ where α is the parameter tuned along the vertical axis multiplying all single pulse areas within a composite pulse protocol. Phase shifts are evaluated mod $\pm k\pi$, $k \in \mathbb{N}$ (see also Ref. [25]). Arrows are pointing pulse area values for a maximum central fringe amplitude (black) or a high-order sensitivity to the accumulated phase shift (red).

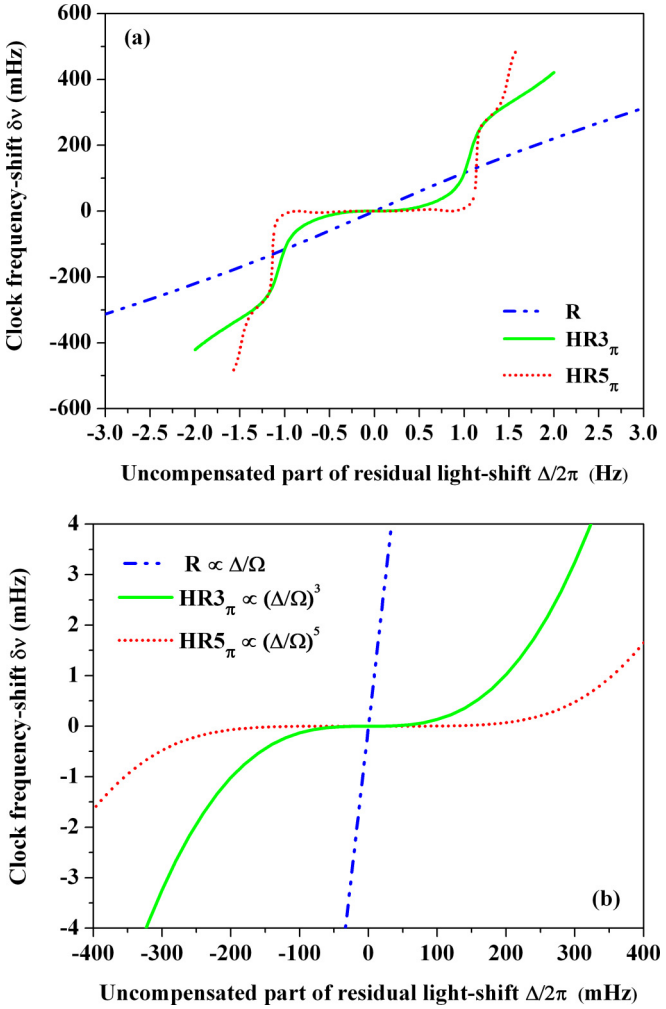

FIG. 5. Central error signal interference frequency-shift ${}^{q}_{p}\widetilde{\Phi}_{gg}/(2\pi T)$ versus residual uncompensated part of the light shift (a) for Ramsey (R) protocol (${}^{1}_{1'}\widetilde{\Phi}_{gg}$ with blue dashed-dot line), HR3$_\pi$ protocol (${}^{2}_{1'}\widetilde{\Phi}_{gg}$ with a continuous green line), and HR5$_\pi$ protocol (${}^{4}_{1'}\widetilde{\Phi}_{gg}$ with a red short-dotted line). (b) Zoom of clock frequency shifts emphasizing the linear dependence $\propto \Delta/\Omega$, the cubic dependence $\propto (\Delta/\Omega)^3$ and the quintic dependence $\propto (\Delta/\Omega)^5$ versus residual uncompensated part of the light-shift $\Delta/2\pi$. Same laser parameters as in Fig. 3 with a fixed pulse area parameter $\alpha = 1$ for all curves.

noted as the HR3$_\pi$ protocol, is based on a sequence of three laser pulses [16]. It relies on replacing the first or the second Ramsey pulse by a combination of two pulses (a composite pulse) including an additional laser phase-step of π. The sequence of five laser pulses ($p = 4'$, $q = 1$ or $p = 1'$, $q = 4$) is a new high-order HR5$_\pi$ protocol including at this time a set of more elaborated composite pulses as $360^\circ_\pi 540^\circ 360^\circ_\pi$ replacing the intermediate 180°_π pulse. For both cases HR3$_\pi$ and HR5$_\pi$, the interference signal calculated using Eq. (14) is shown in Figs. 3(a) and 3(b) versus the clock detuning. The three-pulse protocol generating hyper-Ramsey interferences [Fig. 3(a)] has been successfully applied on the single-ion $^{171}Yb^{+}$ octupole clock demonstrating a relative accuracy of 3×10^{-18} [20]. The composite phase shift related to these configurations is denoted ${}^{q}_{p}\widetilde{\Phi}_{gg}$. To derive the analytical expression of the corresponding clock frequency-shift ${}^{q}_{p}\widetilde{\Phi}/(2\pi T)$, the ERG transformation rules are iterated up to three times generating required $()^{p,q}_{x,y,z}$ elements with $l = 1'$–$3'$; $l = 1$–$3 \in \{4', 4\}$.

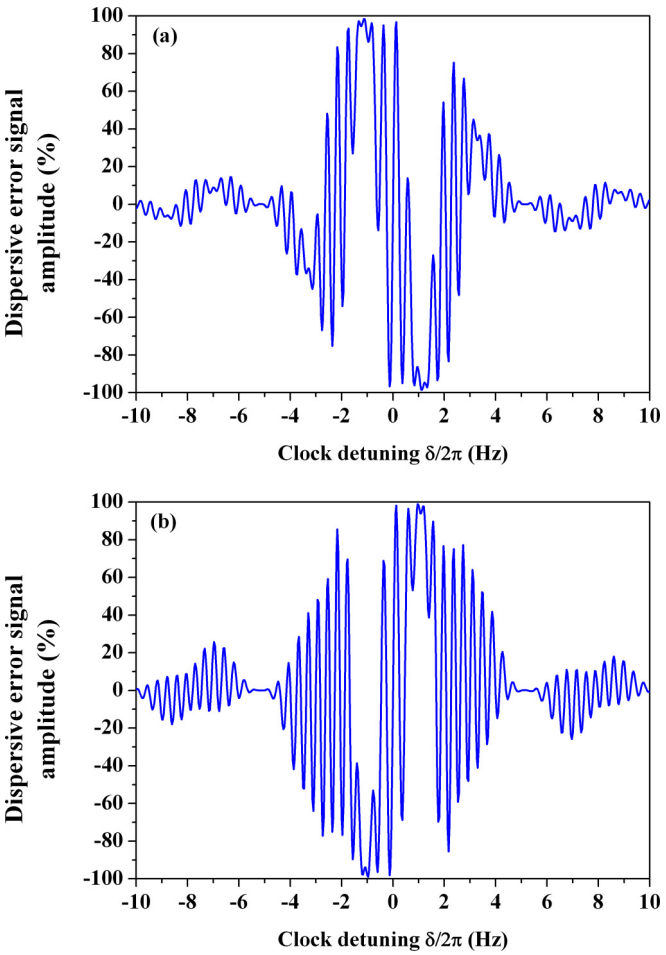

FIG. 6. Examples of dispersive error signals based on ${}^{2}_{2'}C_{gg}$, calculated with Eq. (A13)and applying the ERG transformation through Eq. (A16). (a) $90^{\circ}_{\pm\pi/2}90'^{\circ} \dashv \delta T \vdash 270^{\circ}$, (b) $90^{\circ}_{\pm\pi/2}90'^{\circ} \dashv \delta T \vdash 180^{\circ}_{\pi}90^{\circ}$. The Rabi frequency for all pulses is $\Omega = \pi/2\tau$ where the pulse duration reference is $\tau = 3/16$ s, and the free evolution time is $T = 2$ s.

B. Two-dimensional map optimization of composite pulse protocols

As applications, we consider relevant phase-shifts ${}^{1}_{1'}\widetilde{\Phi}_{gg}$, ${}^{2}_{1'}\widetilde{\Phi}_{gg}$, and ${}^{4}_{1'}\widetilde{\Phi}_{gg}$. Corresponding two-dimensional (2D) diagrams reconstructing the clock frequency-shifts ${}^{2}_{1'}\widetilde{\Phi}_{gg}/(2\pi T)$ and ${}^{4}_{1'}\widetilde{\Phi}_{gg}/(2\pi T)$ versus the residual light shift and pulse area are shown in Figs. 4(a) and 4(b). We choose the amplitude of the frequency shift to be indicated by a color graded scale between -2 and 2 mHz values as in Ref. [24].

A careful investigation of these diagrams allows us to extract some key parameters optimizing the robustness of the clock frequency shift associated with $\mathrm{HR3}_{\pi}$ and $\mathrm{HR5}_{\pi}$ protocols. We are able to explore wide regions of several multiple values of the laser pulse area where the single pulse area reference is introduced as $\Omega\tau = \alpha \times \pi/2\ (\equiv 90^{\circ})$. The error signal amplitude is always maximized for odd values and vanishing for even values of this α parameter. By increasing the pulse area tuning parameter α, the related light-shift correction is increasing quadratically with the Rabi frequency but can still be fully compensated by adjusting the laser frequency step [15]. The clock-frequency-shift compensation can be made more robust by slightly shifting the pulse area parameter from $\alpha = 1, 3$ (black arrow) to $\alpha = 4/3, 8/3$ (red arrows) for the $\mathrm{HR3}_{\pi}$ protocol [black and red arrows are pointing to different pulse area values reported in Fig. 4(a)] These particular pulse areas are strongly upgrading the compensation of the clock frequency shift up to two or three orders of magnitude but are associated with a relative reduction in the central fringe amplitude by $\sim$30%. As an example, injecting a residual light shift of $\Delta/2\pi \sim 200$ mHz with a free evolution time of $T = 2$ s using the $\mathrm{HR3}_{\pi}$ protocol, the composite clock frequency-shift ${}^{2}_{1'}\widetilde{\Phi}_{gg}/(2\pi T)$ drops from 1.3 mHz (for $\alpha = 1$) to -0.043 mHz (for $\alpha = 4/3$) and even -2.5 μHz (for $\alpha = 8/3$) if adjusting carefully the light-shift precompensation. Injecting the same initial residual light-shift with the $\mathrm{HR5}_{\pi}$ protocol gives a clock frequency-shift ${}^{4}_{1'}\widetilde{\Phi}_{gg}/(2\pi \mathrm{T})$ about 0.11 mHz (for $\alpha = 1$) collapsing to 1.5 μHz (for $\alpha = 3$) with no reduction in the signal amplitude.

We note that these specific values of the pulse area are steering the clock frequency shift to locking points offering a better compensation of the systematics synchronized with the laser probe intensity fluctuation when a pulse area modification of a few percent as $\Delta\theta/\theta \equiv \Delta\alpha/\alpha < \pm 5\%$ is tolerated [identified by violet and pink color graded regions in Figs. 4(a) and 4(b) where an abrupt flip is observed between positive and negative clock frequency-shift values of similar amplitude]. As a difference to the $\mathrm{HR3}_{\pi}$ scheme, the $\mathrm{HR5}_{\pi}$ protocol gets exceptional pulse area values where the fringe interference contrast is maximum, and the clock frequency shift exhibits a higher-order dependence to the residual light shift [black and red arrows are pointing to the same pulse area values denoted as exceptional points reported in Fig. 4(b)]. Our new $\mathrm{HR5}_{\pi}$ protocol is simultaneously optimizing the error signal amplitude and the robustness of quantum interferences against probe-induced uncompensated residual light shifts.

Clock frequency shifts of quantum interferences versus the residual light shift are finally simulated and reported in Figs. 5(a) and 5(b) with a reference pulse fixed to $\Omega\tau = \pi/2$ ($\equiv 90^{\circ}$) following the horizontal axis of Fig. 4 taking $\alpha = 1$. Whereas the Ramsey clock frequency shift is a linear function of the residual light shift affecting the quantum states, the cubic sensitivity from a three-pulse scheme turns to collapse to a high-order quintic sensitivity to residual light shifts under a five-pulse protocol as reported in Fig. 5(b).

The required elements needed to calculate ${}^{1}_{1'}\widetilde{\Phi}_{gg}$ are given by

$$
\begin{aligned}
()^{1'}_{x} &= \widehat{n}_{1'_x} \tan\widetilde{\theta}_{1'}, \quad ()^{1}_{x} = \widehat{n}_{1_x} \tan\widetilde{\theta}_{1},\\
()^{1'}_{y} &= \widehat{n}_{1'_y} \tan\widetilde{\theta}_{1'}, \quad ()^{1}_{y} = \widehat{n}_{1_y} \tan\widetilde{\theta}_{1},\\
()^{1'}_{z} &= \widehat{n}_{1'_z} \tan\widetilde{\theta}_{1'}, \quad ()^{1}_{z} = \widehat{n}_{1_z} \tan\widetilde{\theta}_{1}.
\end{aligned}
\tag{17}
$$

By applying Eq. (16), the original Ramsey clock frequency shift reduces to

$$
\begin{aligned}
{}^{1}_{1'}\widetilde{\Phi}_{gg} &= \varphi_1 - \varphi_{1'} + \frac{\delta_{1'}}{\omega_{1'}} \tan\widetilde{\theta}_{1'} + \frac{\delta_1}{\omega_1} \tan\widetilde{\theta}_{1}\\
&= \varphi_1 - \varphi_{1'} + \phi_{1'} + \phi_1,
\end{aligned}
\tag{18}
$$

in accordance with Refs.[19,25,49].

The required elements needed to calculate ${}^{2}_{1'}\widetilde{\Phi}_{gg}$ or ${}^{1}_{2'}\widetilde{\Phi}_{gg}$ are as follows:

$$
\begin{aligned}
()^{2'}_{x} &= \frac{\widehat{n}_{1'_x}\tan\widetilde{\theta}_{1'} + \widehat{n}_{2'_x}\tan\widetilde{\theta}_{2'} + \left(\widehat{n}_{1'_z}\widehat{n}_{2'_y} - \widehat{n}_{1'_y}\widehat{n}_{2'_z}\right)\tan\widetilde{\theta}_{1'}\tan\widetilde{\theta}_{2'}}{1 - \left(n_{1'_x}n_{2'_x} + n_{1'_y}n_{2'_y} + n_{1'_z}n_{2'_z}\right)\tan\widetilde{\theta}_{1'}\tan\widetilde{\theta}_{2'}},\\
()^{2'}_{y} &= \frac{\widehat{n}_{1'_y}\tan\widetilde{\theta}_{1'} + \widehat{n}_{2'_y}\tan\widetilde{\theta}_{2'} + \left(\widehat{n}_{1'_x}\widehat{n}_{2'_z} - \widehat{n}_{1'_z}\widehat{n}_{2'_x}\right)\tan\widetilde{\theta}_{1'}\tan\widetilde{\theta}_{2'}}{1 - \left(n_{1'_x}n_{2'_x} + n_{1'_y}n_{2'_y} + n_{1'_z}n_{2'_z}\right)\tan\widetilde{\theta}_{1'}\tan\widetilde{\theta}_{2'}},\\
()^{2'}_{z} &= \frac{\widehat{n}_{1'_z}\tan\widetilde{\theta}_{1'} + \widehat{n}_{2'_z}\tan\widetilde{\theta}_{2'} + \left(\widehat{n}_{1'_y}\widehat{n}_{2'_x} - \widehat{n}_{1'_x}\widehat{n}_{2'_y}\right)\tan\widetilde{\theta}_{1'}\tan\widetilde{\theta}_{2'}}{1 - \left(n_{1'_x}n_{2'_x} + n_{1'_y}n_{2'_y} + n_{1'_z}n_{2'_z}\right)\tan\widetilde{\theta}_{1'}\tan\widetilde{\theta}_{2'}},
\end{aligned}
\tag{19}
$$

and

$$
\begin{aligned}
()^{2}_{x} &= \frac{\widehat{n}_{1_x}\tan\widetilde{\theta}_{1} + \widehat{n}_{2_x}\tan\widetilde{\theta}_{2} - \left(\widehat{n}_{1_z}\widehat{n}_{2_y} - \widehat{n}_{1_y}\widehat{n}_{2_z}\right)\tan\widetilde{\theta}_{1}\tan\widetilde{\theta}_{2}}{1 - \left(n_{1_x}n_{2_x} + n_{1_y}n_{2_y} + n_{1_z}n_{2_z}\right)\tan\widetilde{\theta}_{1}\tan\widetilde{\theta}_{2}},\\
()^{2}_{y} &= \frac{\widehat{n}_{1_y}\tan\widetilde{\theta}_{1} + \widehat{n}_{2_y}\tan\widetilde{\theta}_{2} - \left(\widehat{n}_{1_x}\widehat{n}_{2_z} - \widehat{n}_{1_z}\widehat{n}_{2_x}\right)\tan\widetilde{\theta}_{1}\tan\widetilde{\theta}_{2}}{1 - \left(n_{1_x}n_{2_x} + n_{1_y}n_{2_y} + n_{1_z}n_{2_z}\right)\tan\widetilde{\theta}_{1}\tan\widetilde{\theta}_{2}},\\
()^{2}_{z} &= \frac{\widehat{n}_{1_z}\tan\widetilde{\theta}_{1} + \widehat{n}_{2_z}\tan\widetilde{\theta}_{2} - \left(\widehat{n}_{1_y}\widehat{n}_{2_x} - \widehat{n}_{1_x}\widehat{n}_{2_y}\right)\tan\widetilde{\theta}_{1}\tan\widetilde{\theta}_{2}}{1 - \left(n_{1_x}n_{2_x} + n_{1_y}n_{2_y} + n_{1_z}n_{2_z}\right)\tan\widetilde{\theta}_{1}\tan\widetilde{\theta}_{2}}.
\end{aligned}
\tag{20}
$$

By fixing $\theta_{2'} \equiv 0$ into Eq. (19) whereas inserting $\widehat{n}_{1_y} = \widehat{n}_{2_y} \equiv 0$ in Eq. (20), the hyper-Ramsey clock frequency shift becomes identical to Ref. [19].

Required elements needed to calculate ${}^{4}_{1'}\widetilde{\Phi}_{gg}$ or ${}^{1}_{4'}\widetilde{\Phi}_{gg}$ are rapidly increasing in size and are not given here. They can be derived applying two times the ERG transformation rules on Eqs. (19) and (20) (see the Appendix section for analytics). This five-pulse protocol has been also derived with the other recursive algorithm [56] following Ref. [4] confirming the accuracy of the plots reported in Figs. 5(a) and 5(b).

IV. CONCLUSION

A SU(2) formulation of hyper-Ramsey interferences with composite phase shifts has been presented. Hyper-clock interrogation protocols and their interferometric dependence to a light shift have been classified by analogy with Pascal's triangle representation of doublet, triplet, and quintet splitting patterns from spin-spin interaction in proton NMR multiplet spectroscopy [63]. Such a representation may ease the search for new and more efficient interrogation protocols of ultranarrow optical clock transitions whereas offering a framework to derive analytically the phase shifts associated with arbitrary laser pulses, showing the remarkable intrinsic robustness introduced in quantum metrology by hyper-qubit clocks. In the present paper, a five-pulse protocol is discovered to be a high-order version of the hyper-Ramsey three-pulse scheme demonstrating a quintic sensitivity to residual probe-induced light shifts with a maximum signal amplitude.

The Pauli-spin model, complementary to analytical tools introduced in Ref. [4] describing hyper-Ramsey-Bordé matter-wave interferometry, uses another recursive algorithm connected to rotation composition rules of unit-quaternions (or versors) algebra in a four-dimensional space [41]. Natural extension to SU(3) composite phase shifts via three-level state interferences (hyper-qutrit clock) may be also explored [64] using a compact representation of Gell-Mann spin matrices [65–67]. Composite phase shifts would certainly be an advantage to qudit multiple rotations exposed to detrimental AC Stark shifts for robust quantum computation [68]. The next generation of quantum clocks will irrevocably bring a relative level of accuracy below 10^{-18} through very long coherence times [69–71], probably supported by robustness against noise with programmable quantum circuit technologies [72,73], quantum nondemolition measurements [74,75] and state entanglement [76]. At this future level of accuracy, hyper-clocks with an optimal control of composite phase shifts should reduce the influence of laser-probe-intensity fluctuations [50] whereas offering an additional toolbox for a fine-tuning control of the optical clock frequency in trapped multi-ion clocks [77] and in optical lattice clocks [78].

This paper in parallel with Ref. [4] should serve as quantum engineering methods to explore cooperative composite pulse protocols [24,79] dedicated to robust control algorithms upgrading performances of optical frequency standards [80], quantum computation with qubits and qudits immune to light shift [68,81], robust quantum sensing [82], and pushing further high-precision laser spectroscopy with cold molecules [83] and cold anti-matter [84].

ACKNOWLEDGMENTS

T.Z.-W. is deeply grateful to Dr. J.-P. Karr, Dr. E. de Clercq, P. M. Cahay, the Wilkowski laboratory teams with Sr(I) and Sr(II) projects for discussion, comments, and criticism. V.I.Y. was supported by the Russian Foundation for Basic Research (Grants No. 20-02-00505 and No. 19-32-90181) and Foundation for the Advancement of Theoretical Physics and Mathematics "BASIS." A.V.T. acknowledges financial support from the Russian Science Foundation through Grant No. 20-12-00081. T.Z.-W. acknowledges Sorbonne Université and MajuLab for supporting a 12 months visiting research associate professorship at center for quantum technologies (CQT) in Singapore. D.W. acknowledges CQT/MoE funding Grant No. R-710-002-016-271, and the NRF/QEP funding Grant No. NRF2021-QEP2-03-P01.

APPENDIX

1. building block for $\tan_p^q \widetilde{\Phi}^{\pm}_{uu'}$

In this Appendix, the decomposition of Eq. (9) from the main text is explicitly provided with Cartesian axis coordinates $\widehat{n}_{p_{x,y,z}}$, $\widehat{n}_{q_{x,y,z}}$, and $\widehat{m}_{x,y,z}$. The interferometric composite phase-shift numerator and denominator can be explicitly developed using the Pauli matrices. For the diagonal phase shift, we obtain the numerator components to build $\{\tan_p^q \widetilde{\Phi}^{\pm}_{gg}\}_N$,

$$\begin{aligned}
\widehat{n}_p \cdot (\overrightarrow{\sigma} \pm \widehat{m}\sigma_0) &= \widehat{n}_{p_z} \pm \left(\widehat{m}_x\widehat{n}_{p_x} + \widehat{m}_y\widehat{n}_{p_y} + \widehat{m}_z\widehat{n}_{p_z}\right),\\
\widehat{n}_q \cdot (\overrightarrow{\sigma} \pm \widehat{m}\sigma_0) &= \widehat{n}_{q_z} \pm \left(\widehat{m}_x\widehat{n}_{q_x} + \widehat{m}_y\widehat{n}_{q_y} + \widehat{m}_z\widehat{n}_{q_z}\right),\\
(\widehat{n}_p \times \widehat{n}_q) \cdot (\overrightarrow{\sigma} \mp \widehat{m}\sigma_0) &= \widehat{n}_{p_x}\widehat{n}_{q_y} - \widehat{n}_{q_x}\widehat{n}_{p_y}\\
&\quad \mp \widehat{m}_x\left(\widehat{n}_{q_z}\widehat{n}_{p_y} - \widehat{n}_{q_y}\widehat{n}_{p_z}\right)\\
&\quad \mp \widehat{m}_y\left(\widehat{n}_{q_x}\widehat{n}_{p_z} - \widehat{n}_{q_z}\widehat{n}_{p_x}\right)\\
&\quad \mp \widehat{m}_z\left(\widehat{n}_{p_x}\widehat{n}_{q_y} - \widehat{n}_{q_x}\widehat{n}_{p_y}\right),
\end{aligned} \tag{A1}$$

and the denominator components to build $\{\tan_p^q \widetilde{\Phi}^{\pm}_{gg}\}_D$,

$$\begin{aligned}
\sigma_0 \pm \widehat{m}\overrightarrow{\sigma} &= 1 \pm \widehat{m}_z,\\
[\widehat{n}_p \times \widehat{m}] \cdot \overrightarrow{\sigma} &= \widehat{m}_y\widehat{n}_{p_x} - \widehat{m}_x\widehat{n}_{p_y},\\
[\widehat{n}_q \times \widehat{m}] \cdot \overrightarrow{\sigma} &= \widehat{m}_y\widehat{n}_{q_x} - \widehat{m}_x\widehat{n}_{q_y},\\
(\widehat{n}_p \cdot \widehat{n}_q)_{\widehat{m},\overrightarrow{\sigma}} &= \widehat{n}_{p_x}\widehat{n}_{q_x} + \widehat{n}_{p_y}\widehat{n}_{q_y} + \widehat{n}_{p_z}\widehat{n}_{q_z}\\
&\quad \mp \widehat{m}_z\left(\widehat{n}_{p_x}\widehat{n}_{q_x} + \widehat{n}_{p_y}\widehat{n}_{q_y} + \widehat{n}_{p_z}\widehat{n}_{q_z}\right)\\
&\quad \pm \widehat{n}_{q_z}\left(\widehat{m}_x\widehat{n}_{p_x} + \widehat{m}_y\widehat{n}_{p_y} + \widehat{m}_z\widehat{n}_{p_z}\right)\\
&\quad \pm \widehat{n}_{p_z}\left(\widehat{m}_x\widehat{n}_{q_x} + \widehat{m}_y\widehat{n}_{q_y} + \widehat{m}_z\widehat{n}_{q_z}\right).
\end{aligned} \tag{A2}$$

For the off-diagonal complex phase shift, we obtain the numerator components for $\{\tan_p^q \widetilde{\Phi}^{\pm}_{eg}\}_N$,

$$\begin{aligned}
\widehat{n}_p \cdot (\overrightarrow{\sigma} \pm \widehat{m}\sigma_0) &= \widehat{n}_{p_x} + i\widehat{n}_{p_y},\\
\widehat{n}_q \cdot (\overrightarrow{\sigma} \pm \widehat{m}\sigma_0) &= \widehat{n}_{q_x} + i\widehat{n}_{q_y},\\
(\widehat{n}_p \times \widehat{n}_q) \cdot (\overrightarrow{\sigma} \mp \widehat{m}\sigma_0) &= \left(\widehat{n}_{q_y}\widehat{n}_{p_z} - \widehat{n}_{q_z}\widehat{n}_{p_y}\right)\\
&\quad + i\left(\widehat{n}_{q_z}\widehat{n}_{p_x} - \widehat{n}_{q_x}\widehat{n}_{p_z}\right),
\end{aligned} \tag{A3}$$

and the denominator components for $\{\tan_p^q \widetilde{\Phi}^{\pm}_{eg}\}_D$,

$$\begin{aligned}
\sigma_0 \pm \widehat{m}\overrightarrow{\sigma} &= \pm(\widehat{m}_x + i\widehat{m}_y),\\
[\widehat{n}_p \times \widehat{m}] \cdot \overrightarrow{\sigma} &= \left(\widehat{m}_z\widehat{n}_{p_y} - \widehat{m}_y\widehat{n}_{p_z}\right) + i\left(\widehat{m}_x\widehat{n}_{p_z} - \widehat{m}_z\widehat{n}_{p_x}\right),\\
[\widehat{n}_q \times \widehat{m}] \cdot \overrightarrow{\sigma} &= \left(\widehat{m}_z\widehat{n}_{q_y} - \widehat{m}_y\widehat{n}_{q_z}\right) + i\left(\widehat{m}_x\widehat{n}_{q_z} - \widehat{m}_z\widehat{n}_{q_x}\right),\\
(\widehat{n}_p \cdot \widehat{n}_q)_{\widehat{m},\overrightarrow{\sigma}} &= \mp(\widehat{m}_x + i\widehat{m}_y)\left(\widehat{n}_{p_x}\widehat{n}_{q_x} + \widehat{n}_{p_y}\widehat{n}_{q_y} + \widehat{n}_{p_z}\widehat{n}_{q_z}\right)\\
&\quad \pm \left(\widehat{n}_{q_x} + i\widehat{n}_{q_y}\right)\left(\widehat{m}_x\widehat{n}_{p_x} + \widehat{m}_y\widehat{n}_{p_y} + \widehat{m}_z\widehat{n}_{p_z}\right)\\
&\quad \pm \left(\widehat{n}_{p_x} + i\widehat{n}_{p_y}\right)\left(\widehat{m}_x\widehat{n}_{q_x} + \widehat{m}_y\widehat{n}_{q_y} + \widehat{m}_z\widehat{n}_{q_z}\right),
\end{aligned} \tag{A4}$$

where N, D stands for the numerator and the denominator of the quantity $\tan_p^q \widetilde{\Phi}^{\pm}_{uu'}$ and all elements have to be associated with $\tan\widetilde{\theta}_p$ and $\tan\widetilde{\theta}_q$. Now, we proceed by fixing the orientation axis $\widehat{m} = (0, 0, 1)$ as in the main text. We explicitly derive the diagonal phase-shift expressions ${}^q_p\widetilde{\Phi}^{\pm}_{gg}$ with the help of Eqs. (A1) and (A2),

$$\begin{aligned}
\tan_p^q \widetilde{\Phi}^{+}_{gg} &= \frac{\widehat{n}_{p_z}\tan\widetilde{\theta}_p + \widehat{n}_{q_z}\tan\widetilde{\theta}_q}{1 - \widehat{n}_{p_z}\widehat{n}_{q_z}\tan\widetilde{\theta}_p\tan\widetilde{\theta}_q},\\
\tan_p^q \widetilde{\Phi}^{-}_{gg} &= \frac{\widehat{n}_{p_y}\widehat{n}_{q_x} - \widehat{n}_{p_x}\widehat{n}_{q_y}}{\widehat{n}_{p_x}\widehat{n}_{q_x} + \widehat{n}_{p_y}\widehat{n}_{q_y}}.
\end{aligned} \tag{A5}$$

Using normalized parameters from the main text $\widehat{n}_{l_x} \equiv \frac{\Omega_l}{\omega_l}\cos\varphi_l$, $\widehat{n}_{l_y} \equiv \frac{\Omega_l}{\omega_l}\sin\varphi_l$, and $\widehat{n}_{l_z} \equiv \frac{\delta_l}{\omega_l}$ with $(l = p, q)$, we obtain with Eq. (16), the overall Ramsey phase-shift ${}^q_p\widetilde{\Phi}_{gg}$,

$$\begin{aligned}
{}^q_p\widetilde{\Phi}_{gg} &= \varphi_q - \varphi_p + \phi_p + \phi_q\\
&= \varphi_1 - \varphi_{1'} + \phi_{1'} + \phi_1,
\end{aligned} \tag{A6}$$

where we use $\phi_l = \frac{\delta_l}{\omega_l}\tan\widetilde{\theta}_l$. Indeed, we have recovered the Ramsey phase shift by fixing $p = 1'$ and $q = 1$ as two single pulses.

2. $()^{4'}_{x,y,z}$ and $()^{4}_{x,y,z}$ elements for ${}^4_{1'}\widetilde{\mathbf{\Phi}}_{gg}$ and ${}^1_{4'}\widetilde{\mathbf{\Phi}}_{gg}$

The ERG transformation through Eq. (15) is applied twice on numerator and denominator elements from Eqs. (19) and (20) with $p = 4'$, $q = 4$ pulses.

The transformation gives for the set of $p = 4'$ composite pulses,

$$\begin{aligned}
\widehat{n}_{2'}\tan\widetilde{\theta}_{2'} &\mapsto \frac{{}^{3'}_{2'}\widehat{N}_+ - {}^{3'}_{2'}\widehat{N}_\times}{1 - {}^{3'}_{2'}\widehat{N}^0_\bullet},\\
\widehat{n}_{3'}\tan\widetilde{\theta}_{3'} &\mapsto \frac{{}^{4'}_{3'}\widehat{N}_+ - {}^{4'}_{3'}\widehat{N}_\times}{1 - {}^{4'}_{3'}\widehat{N}^0_\bullet}.
\end{aligned} \tag{A7}$$

The transformation gives for the set of $q = 4$ composite pulses,

$$\begin{aligned}
\widehat{n}_2\tan\widetilde{\theta}_2 &\mapsto \frac{{}^{3}_{2}\widehat{N}_+ + {}^{3}_{2}\widehat{N}_\times}{1 - {}^{3}_{2}\widehat{N}^0_\bullet},\\
\widehat{n}_3\tan\widetilde{\theta}_3 &\mapsto \frac{{}^{4}_{3}\widehat{N}_+ + {}^{4}_{3}\widehat{N}_\times}{1 - {}^{4}_{3}\widehat{N}^0_\bullet}.
\end{aligned} \tag{A8}$$

New expressions for components are, thus,

$$\begin{aligned}
\widehat{n}_{2'_x}\tan\widetilde{\theta}_{2'} &\mapsto \frac{\widehat{n}_{2'_x}\tan\widetilde{\theta}_{2'} + \widehat{n}_{3'_x}\tan\widetilde{\theta}_{3'} + \left(\widehat{n}_{2'_z}\cdot\widehat{n}_{3'_y}\tan\widetilde{\theta}_{3'} - \widehat{n}_{2'_y}\cdot\widehat{n}_{3'_z}\tan\widetilde{\theta}_{3'}\right)\tan\widetilde{\theta}_{2'}}{1 - \left(\widehat{n}_{2'_x}\cdot\widehat{n}_{3'_x}\tan\widetilde{\theta}_{3'} + \widehat{n}_{2'_y}\cdot\widehat{n}_{3'_y}\tan\widetilde{\theta}_{3'} + \widehat{n}_{2'_z}\cdot\widehat{n}_{3'_z}\tan\widetilde{\theta}_{3'}\right)\tan\widetilde{\theta}_{2'}},\\
\widehat{n}_{2'_y}\tan\widetilde{\theta}_{2'} &\mapsto \frac{\widehat{n}_{2'_y}\tan\widetilde{\theta}_{2'} + \widehat{n}_{3'_y}\tan\widetilde{\theta}_{3'} + \left(\widehat{n}_{2'_x}\cdot\widehat{n}_{3'_z}\tan\widetilde{\theta}_{3'} - \widehat{n}_{2'_z}\cdot\widehat{n}_{3'_x}\tan\widetilde{\theta}_{3'}\right)\tan\widetilde{\theta}_{2'}}{1 - \left(\widehat{n}_{2'_x}\cdot\widehat{n}_{3'_x}\tan\widetilde{\theta}_{3'} + \widehat{n}_{2'_y}\cdot\widehat{n}_{3'_y}\tan\widetilde{\theta}_{3'} + \widehat{n}_{2'_z}\cdot\widehat{n}_{3'_z}\tan\widetilde{\theta}_{3'}\right)\tan\widetilde{\theta}_{2'}},\\
\widehat{n}_{2'_z}\tan\widetilde{\theta}_{2'} &\mapsto \frac{\widehat{n}_{2'_z}\tan\widetilde{\theta}_{2'} + \widehat{n}_{3'_z}\tan\widetilde{\theta}_{3'} + \left(\widehat{n}_{2'_y}\cdot\widehat{n}_{3'_x}\tan\widetilde{\theta}_{3'} - \widehat{n}_{2'_x}\cdot\widehat{n}_{3'_y}\tan\widetilde{\theta}_{3'}\right)\tan\widetilde{\theta}_{2'}}{1 - \left(\widehat{n}'_{2_x}\cdot\widehat{n}_{3'_x}\tan\widetilde{\theta}_{3'} + \widehat{n}_{2'_y}\cdot\widehat{n}_{3'_y}\tan\widetilde{\theta}_{3'} + \widehat{n}_{2'_z}\cdot\widehat{n}_{3'_z}\tan\widetilde{\theta}_{3'}\right)\tan\widetilde{\theta}_{2'}},
\end{aligned} \tag{A9}$$

where $\widehat{n}_{3'_{x,y,z}} \tan\widetilde{\theta}_{3'}$ axial components are replaced by

$$\begin{aligned}
\widehat{n}_{3'_x}\tan\widetilde{\theta}_{3'} &\mapsto \frac{\widehat{n}_{3'_x}\tan\widetilde{\theta}_{3'}+\widehat{n}_{4'_x}\tan\widetilde{\theta}_{4'}+\left(\widehat{n}_{3'_z}\cdot\widehat{n}_{4'_y}\tan\widetilde{\theta}_{4'}-\widehat{n}_{3'_y}\cdot\widehat{n}_{4'_z}\tan\widetilde{\theta}_{4'}\right)\tan\widetilde{\theta}_{3'}}{1-\left(\widehat{n}_{3'_x}\cdot\widehat{n}_{4'_x}\tan\widetilde{\theta}_{4'}+\widehat{n}_{3'_y}\cdot\widehat{n}_{4'_y}\tan\widetilde{\theta}_{4'}+\widehat{n}_{3'_z}\cdot\widehat{n}_{4'_z}\tan\widetilde{\theta}_{4'}\right)\tan\widetilde{\theta}_{3'}},\\
\widehat{n}_{3'_y}\tan\widetilde{\theta}_{3'} &\mapsto \frac{\widehat{n}_{3'_y}\tan\widetilde{\theta}_{3'}+\widehat{n}_{4'_y}\tan\widetilde{\theta}_{4'}+\left(\widehat{n}_{3'_x}\cdot\widehat{n}_{4'_z}\tan\widetilde{\theta}_{4'}-\widehat{n}_{3'_z}\cdot\widehat{n}_{4'_x}\tan\widetilde{\theta}_{4'}\right)\tan\widetilde{\theta}_{3'}}{1-\left(\widehat{n}_{3'_x}\cdot\widehat{n}_{4'_x}\tan\widetilde{\theta}_{4'}+\widehat{n}_{3'_y}\cdot\widehat{n}_{4'_y}\tan\widetilde{\theta}_{4'}+\widehat{n}_{3'_z}\cdot\widehat{n}_{4'_z}\tan\widetilde{\theta}_{4'}\right)\tan\widetilde{\theta}_{3'}},\\
\widehat{n}_{3'_z}\tan\widetilde{\theta}_{3'} &\mapsto \frac{\widehat{n}_{3'_z}\tan\widetilde{\theta}_{3'}+\widehat{n}_{4'_z}\tan\widetilde{\theta}_{4'}+\left(\widehat{n}_{3'_y}\cdot\widehat{n}_{4'_x}\tan\widetilde{\theta}_{4'}-\widehat{n}_{3'_x}\cdot\widehat{n}_{4'_y}\tan\widetilde{\theta}_{4'}\right)\tan\widetilde{\theta}_{3'}}{1-\left(\widehat{n}_{3'_x}\cdot\widehat{n}_{4'_x}\tan\widetilde{\theta}_{4'}+\widehat{n}_{3'_y}\cdot\widehat{n}_{4'_y}\tan\widetilde{\theta}_{4'}+\widehat{n}_{3'_z}\cdot\widehat{n}_{4'_z}\tan\widetilde{\theta}_{4'}\right)\tan\widetilde{\theta}_{3'}},
\end{aligned} \tag{A10}$$

and

$$\begin{aligned}
\widehat{n}_{2_x}\tan\widetilde{\theta}_2 &\mapsto \frac{\widehat{n}_{2_x}\tan\widetilde{\theta}_2+\widehat{n}_{3_x}\tan\widetilde{\theta}_3-\left(\widehat{n}_{2_z}\cdot\widehat{n}_{3_y}\tan\widetilde{\theta}_3-\widehat{n}_{2_y}\cdot\widehat{n}_{3_z}\tan\widetilde{\theta}_3\right)\tan\widetilde{\theta}_2}{1-\left(\widehat{n}_{2_x}\cdot\widehat{n}_{3_x}\tan\widetilde{\theta}_3+\widehat{n}_{2_y}\cdot\widehat{n}_{3_y}\tan\widetilde{\theta}_3+\widehat{n}_{2_z}\cdot\widehat{n}_{3_z}\tan\widetilde{\theta}_3\right)\tan\widetilde{\theta}_2},\\
\widehat{n}_{2_y}\tan\widetilde{\theta}_2 &\mapsto \frac{\widehat{n}_{2_y}\tan\widetilde{\theta}_2+\widehat{n}_{3_y}\tan\widetilde{\theta}_3-\left(\widehat{n}_{2_x}\cdot\widehat{n}_{3_z}\tan\widetilde{\theta}_3-\widehat{n}_{2_z}\cdot\widehat{n}_{3_x}\tan\widetilde{\theta}_3\right)\tan\widetilde{\theta}_2}{1-\left(\widehat{n}_{2_x}\cdot\widehat{n}_{3_x}\tan\widetilde{\theta}_3+\widehat{n}_{2_y}\cdot\widehat{n}_{3_y}\tan\widetilde{\theta}_3+\widehat{n}_{2_z}\cdot\widehat{n}_{3_z}\tan\widetilde{\theta}_3\right)\tan\widetilde{\theta}_2},\\
\widehat{n}_{2_z}\tan\widetilde{\theta}_2 &\mapsto \frac{\widehat{n}_{2_z}\tan\widetilde{\theta}_2+\widehat{n}_{3_z}\tan\widetilde{\theta}_3-\left(\widehat{n}_{2_y}\cdot\widehat{n}_{3_x}\tan\widetilde{\theta}_3-\widehat{n}_{2_x}\cdot\widehat{n}_{3_y}\tan\widetilde{\theta}_3\right)\tan\widetilde{\theta}_2}{1-\left(\widehat{n}_{2_x}\cdot\widehat{n}_{3_x}\tan\widetilde{\theta}_3+\widehat{n}_{2_y}\cdot\widehat{n}_{3_y}\tan\widetilde{\theta}_3+\widehat{n}_{2_z}\cdot\widehat{n}_{3_z}\tan\widetilde{\theta}_3\right)\tan\widetilde{\theta}_2},
\end{aligned} \tag{A11}$$

where $\widehat{n}_{3_{x,y,z}} \tan\widetilde{\theta}_3$ axial components are replaced by

$$\begin{aligned}
\widehat{n}_{3_x}\tan\widetilde{\theta}_3 &\mapsto \frac{\widehat{n}_{3_x}\tan\widetilde{\theta}_3+\widehat{n}_{4_x}\tan\widetilde{\theta}_4-\left(\widehat{n}_{3_z}\cdot\widehat{n}_{4_y}\tan\widetilde{\theta}_4-\widehat{n}_{3_y}\cdot\widehat{n}_{4_z}\tan\widetilde{\theta}_4\right)\tan\widetilde{\theta}_3}{1-\left(\widehat{n}_{3_x}\cdot\widehat{n}_{4_x}\tan\widetilde{\theta}_4+\widehat{n}_{3_y}\cdot\widehat{n}_{4_y}\tan\widetilde{\theta}_4+\widehat{n}_{3_z}\cdot\widehat{n}_{4_z}\tan\widetilde{\theta}_4\right)\tan\widetilde{\theta}_3},\\
\widehat{n}_{3_y}\tan\widetilde{\theta}_3 &\mapsto \frac{\widehat{n}_{3_y}\tan\widetilde{\theta}_3+\widehat{n}_{4_y}\tan\widetilde{\theta}_4-\left(\widehat{n}_{3_x}\cdot\widehat{n}_{4_z}\tan\widetilde{\theta}_4-\widehat{n}_{3_z}\cdot\widehat{n}_{4_x}\tan\widetilde{\theta}_4\right)\tan\widetilde{\theta}_3}{1-\left(\widehat{n}_{3_x}\cdot\widehat{n}_{4_x}\tan\widetilde{\theta}_4+\widehat{n}_{3_y}\cdot\widehat{n}_{4_y}\tan\widetilde{\theta}_4+\widehat{n}_{3_z}\cdot\widehat{n}_{4_z}\tan\widetilde{\theta}_4\right)\tan\widetilde{\theta}_3},\\
\widehat{n}_{3_z}\tan\widetilde{\theta}_3 &\mapsto \frac{\widehat{n}_{3_z}\tan\widetilde{\theta}_3+\widehat{n}_{4_z}\tan\widetilde{\theta}_4-\left(\widehat{n}_{3_y}\cdot\widehat{n}_{4_x}\tan\widetilde{\theta}_4-\widehat{n}_{3_x}\cdot\widehat{n}_{4_y}\tan\widetilde{\theta}_4\right)\tan\widetilde{\theta}_3}{1-\left(\widehat{n}_{3_x}\cdot\widehat{n}_{4_x}\tan\widetilde{\theta}_4+\widehat{n}_{3_y}\cdot\widehat{n}_{4_y}\tan\widetilde{\theta}_4+\widehat{n}_{3_z}\cdot\widehat{n}_{4_z}\tan\widetilde{\theta}_4\right)\tan\widetilde{\theta}_3}.
\end{aligned} \tag{A12}$$

Phase-shift expressions ${}^{4}_{1'}\widetilde{\Phi}_{gg}$ and ${}^{1}_{4'}\widetilde{\Phi}_{gg}$ can, thus, be analytically obtained encapsulating Eq. (A10) with Eq. (A10) and Eq. (A11) with Eq. (A12) into Eqs. (19) and (20).

3. Spinor interferences with composite pulses

We apply our ERG algorithm following Eq. (13) to derive transition probabilities of composite spinor interferences based on Eq. (5). We use a quantization axis projection with $\widehat{m} = (0, 0, 1)$ leading to $\widetilde{\theta}_{m_z} = \delta T/2$. We first derive the Ramsey formula with two pulses based on the coefficient ${}^{1}_{1'}C_{gg}$ as follows:

$$\begin{aligned}
{}^{1}_{1'}C_{gg} &= {}^{1}_{1'}\widetilde{C}^{+}_{gg}e^{i{}^{1}_{1'}\widetilde{\Phi}^{+}_{gg}}e^{i\widetilde{\theta}_{m_z}} + {}^{1}_{1'}\widetilde{C}^{-}_{gg}e^{i{}^{1}_{1'}\widetilde{\Phi}^{-}_{gg}}e^{-i\widetilde{\theta}_{m_z}},\\
{}^{1}_{1'}\widetilde{C}^{\pm}_{gg} &= \frac{1}{2}(\cos\widetilde{\theta}_{1'}\cos\widetilde{\theta}_1)\,{}^{1}_{1'}C^{\pm}\sqrt{1+\tan^2\left({}^{1}_{1'}\widetilde{\Phi}^{\pm}_{gg}\right)},
\end{aligned} \tag{A13}$$

where phase shifts are given by

$$\begin{aligned}
{}^{1}_{1'}\widetilde{\Phi}^{+}_{gg} &= \arctan\left[\frac{\widehat{n}_{1'_z}\tan\widetilde{\theta}_{1'}+\widehat{n}_{1_z}\tan\widetilde{\theta}_1}{1-\widehat{n}_{1'_z}\widehat{n}_{1_z}\tan\widetilde{\theta}_{1'}\tan\widetilde{\theta}_1}\right]\\
{}^{1}_{1'}\widetilde{\Phi}^{-}_{gg} &= \arctan\left[\frac{\left(\widehat{n}_{1'_y}\widehat{n}_{1_x}-\widehat{n}_{1'_x}\widehat{n}_{1_y}\right)\tan\widetilde{\theta}_{1'}\tan\widetilde{\theta}_1}{\left(\widehat{n}_{1'_x}\widehat{n}_{1_x}+\widehat{n}_{1'_y}\widehat{n}_{1_y}\right)\tan\widetilde{\theta}_{1'}\tan\widetilde{\theta}_1}\right]
\end{aligned} \tag{A14}$$

and,

$$\begin{aligned}
{}^{1}_{1'}C^{+} &= 2-2\widehat{n}_{1'_z}\tan\widetilde{\theta}_{1'}\cdot\widehat{n}_{1_z}\tan\widetilde{\theta}_1,\\
{}^{1}_{1'}C^{-} &= -2\widehat{n}_{1'_x}\tan\widetilde{\theta}_{1'}\cdot\widehat{n}_{1_x}\tan\widetilde{\theta}_1-2\widehat{n}_{1'_y}\tan\widetilde{\theta}_{1'}\cdot\widehat{n}_{1_y}\tan\widetilde{\theta}_1.
\end{aligned} \tag{A15}$$

We now proceed with our ERG algorithm to obtain coefficients of the ${}^{2}_{2'}C_{gg}$ amplitude of transition using $p = 2'$ pulses on the left arm and $q = 2$ pulses on the right arm of the spectroscopic pulse scheme. We get

$$\begin{aligned}
\cos\widetilde{\theta}_{1'} &\mapsto \cos\widetilde{\theta}_{1'}\cos\widetilde{\theta}_{2'}(1-\widehat{n}_{1'}\tan\widetilde{\theta}_{1'}\cdot\widehat{n}_{2'}\tan\widetilde{\theta}_{2'}),\\
\cos\widetilde{\theta}_1 &\mapsto \cos\widetilde{\theta}_1\cos\widetilde{\theta}_2(1-\widehat{n}_1\tan\widetilde{\theta}_1\cdot\widehat{n}_2\tan\widetilde{\theta}_2),\\
\widehat{n}_{1'_{x,y,z}}\tan\widetilde{\theta}_{1'} &\mapsto ()^{2'}_{x,y,z},\\
\widehat{n}_{1_{x,y,z}}\tan\widetilde{\theta}_1 &\mapsto ()^{2}_{x,y,z},\\
{}^{1}_{1'}\widetilde{\Phi}^{\pm}_{gg} &\mapsto {}^{2}_{2'}\widetilde{\Phi}^{\pm}_{gg},
\end{aligned} \tag{A16}$$

where modified elements $()^{2'}_{x,y,z}$ and $()^{2}_{x,y,z}$ are given by Eqs. (19) and (20). We have plotted two examples of arbitrary composite spinor interferences based on four pulses versus the clock detuning in Fig. 6 .

[1] N. F. Ramsey, A new molecular beam resonance method, Phys. Rev. **76**, 996 (1949).

[2] N. F. Ramsey, A molecular beam resonance method with separated oscillating fields, Phys. Rev. **78**, 695 (1950).

[3] N. F. Ramsey, *Molecular Beams* (Oxford University Press, Oxford, 1956).

[4] T. Zanon-Willette, D. Wilkowski, R. Lefevre, A. V. Taichenachev, and V. I. Yudin, *Generalized hyper-Ramsey-Bordé matter-wave interferometry: quantum engineering of robust atomic sensors with composite pulses*, arXiv:2202.06296.

[5] N. F. Ramsey and H. B. Silsbee, Phase shifts in the molecular beam method of separated oscillating fields, Phys. Rev. **84**, 506 (1951).

[6] N. F. Ramsey, Molecular beam resonances in oscillatory fields of nonuniform amplitudes and phases, Phys. Rev. **109**, 822 (1958).

[7] L. Essen and J. V. L. Parry, An atomic standard of frequency and time interval: A cæsium resonator, Nature (London) **176**, 280 (1955).

[8] A. Clairon, C. Salomon, S. Guellati, and W. D. Phillips, Ramsey resonance in a zacharias fountain, Europhys. Lett. **16**, 165 (1991).

[9] N. F. Ramsey, Experiments with separated oscillatory fields and hydrogen masers, Rev. Mod. Phys. **62**, 541 (1990).

[10] S. Haroche and J.-M. Raimond, *Exploring the Quantum, Atoms, Cavities, and Photons* (Oxford University Press, Oxford, 2006).

[11] S. Gleyzes, S. Kuhr, C. Guerlin, J. Bernu, S. Deléglise, U. Busk Hoff, M. Brune, J.-M. Raimond, and S. Haroche, Quantum jumps of light recording the birth and death of a photon in a cavity, Nature (London) **446**, 297 (2007).

[12] S. Haroche, Nobel Lecture: Controlling photons in a box and exploring the quantum to classical boundary, Rev. Mod. Phys. **85**, 1083 (2013).

[13] K. C. McCormick, J. Keller, S. C. Burd, D. J. Wineland, A. C. Wilson, and D. Leibfried, Quantum-enhanced sensing of a single-ion mechanical oscillator, Nature (London) **572**, 86 (2019).

[14] P. Krantz, F. Yan, T. P. Orlando, S. Gustavsson, and W. D. Oliver, A quantum engineer's guide to superconducting qubits, Appl. Phys. Rev. **6**, 021318 (2019).

[15] A. V. Taichenachev, V. I. Yudin, C. W. Oates, Z. W. Barber., N. D. Lemke, A. D. Ludlow, U. Sterr, C. Lisdat, and F. Riehle, Compensation of field-induced frequency shifts in ramsey spectroscopy of optical clock transitions, JETP. Lett. **90**, 713 (2010).

[16] V. I. Yudin, A. V. Taichenachev, C. W. Oates, Z. W. Barber, N. D. Lemke, A. D. Ludlow, U. Sterr, C. Lisdat, and F. Riehle, Hyper-Ramsey spectroscopy of optical clock transitions, Phys. Rev. A **82**, 011804(R) (2010).

[17] N. Huntemann, B. Lipphardt, M. Okhapkin, C. Tamm, E. Peik, A. V. Taichenachev, and V. I. Yudin, Generalized Ramsey Excitation Scheme with Suppressed Light Shift, Phys. Rev. Lett. **109**, 213002 (2012).

[18] A. V. Taichenachev, V. I. Yudin, and S. N. Bagayev, Recent advances in precision spectroscopy of ultracold atoms and ions, J. Phys.: Conf. Ser. **793**, 012027 (2017).

[19] T. Zanon-Willette, V. I. Yudin, and A. V. Taichenachev, Generalized hyper-Ramsey resonance with separated oscillating fields, Phys. Rev. A **92**, 023416 (2015).

[20] N. Huntemann, C. Sanner, B. Lipphardt, Chr. Tamm, and E. Peik, Single-Ion Atomic Clock with 3×10^{-18} Systematic Uncertainty, Phys. Rev. Lett. **116**, 063001 (2016).

[21] T. Zanon-Willette, R. Lefevre, R. Metzdorff, N. Sillitoe, S. Almonacil, M. Minissale, E. de Clercq, A. V. Taichenachev, V. I. Yudin, and E. Arimondo, Composite laser-pulses spectroscopy for high-accuracy optical clocks: A review of recent progress and perspectives, Rep. Prog. Phys. **81**, 094401 (2018).

[22] K. S. Tabatchikova, A. V. Taichenachev, and V. I. Yudin, Generalized Ramsey scheme for precision spectroscopy of ultracold atoms and ions: Inclusion of a finite laser line width and spontaneous relaxation of the atomic levels, JETP Lett. **97**, 311 (2013).

[23] V. I. Yudin, A. V. Taichenachev, M. Yu. Basaleev, and T. Zanon-Willette, Synthetic Frequency Protocol in the Ramsey Spectroscopy of Clock Transitions, Phys. Rev. A **94**, 052505 (2016).

[24] T. Zanon-Willette, R. Lefevre, A. V. Taichenachev, and V. I. Yudin, Universal interrogation protocol with zero probe-field-induced frequency shift for quantum clocks and high-accuracy spectroscopy, Phys. Rev. A **96**, 023408 (2017).

[25] T. Zanon-Willette, A. V. Taichenachev, and V. I. Yudin, Generalised hyper-Ramsey resonance with spinors, Quantum Electron. **49**, 278 (2019).

[26] L. M. K. Vandersypen and I. L. Chuang, NMR techniques for quantum control and computation, Rev. Mod. Phys. **76**, 1037 (2005).

[27] J. A. Jones, Quantum computing with NMR, Prog. Nucl. Magn. Reson. Spectrosc. **59**, 91 (2011).

[28] K. R. Brown and J. T. Merrill, Quantum Information and Computation for Chemistry, *Progress in Compensating Pulse Sequences for Quantum Computation* (John Wiley and Sons, 2014), p. 241.

[29] B. T. Torosov and N. V. Vitanov, Composite pulses with errant phases, Phys. Rev. A **100**, 023410 (2019).

[30] B. T. Torosov and N. V. Vitanov, Experimental demonstration of composite pulses on IBM's quantum computer, arXiv:2202.09647.

[31] W. Pauli Jr., On the quantum mechanics of magnetic electrons, Z. Phys. **43**, 601 (1927).

[32] I. I. Rabi, N. F. Ramsey, and J. Schwinger, Use of rotating coordinates in magnetic resonance problems, Rev. Mod. Phys. **26**, 167 (1954).

[33] L. Euler, Problema algebraicum ob affectiones prorsus singulares memorabile, Novi Comm. Acad. Sci. Petropolitanae **15**, 75 (1770).

[34] O. Rodrigues, Des lois géométriques qui régissent les déplacements d'un système solide dans l'espace, et de la variation des coordonnées provenant de ces déplacements considérés indépendants des causes qui peuvent les produire, J. Math. Pure Appl. **5**, 380 (1840).

[35] J. Willard Gibbs, and E. B. Wilson, *Vector Analysis* (Scribner, New York, 1901).

[36] S. J. Dai, Euler-Rodrigues formula variations, quaternion conjugation and intrinsic connections, Mech. Mach. Theory **92**, 144 (2015).

[37] A. G. Valdenebro, Visualizing rotations and composition of rotations with the Rodrigues vector, Eur. J. Phys. **37**, 065001 (2016).

[38] M. Levitt, Composite pulses, Prog. Nucl. Magn. Reson. Spectrosc. **18**, 61 (1986).

[39] D. J. Siminovitch, Rotations in NMR: Part I. Euler-Rodrigues parameters and quaternions, Concepts Magn. Reson. **9**, 149 (1997).

[40] D. J. Siminovitch, Rotations in NMR: Part II. Applications of the Euler-Rodrigues parameters, Concepts Magn. Reson. **9**, 211 (1997).

[41] S. L. Altmann, *Rotations, Quaternions and Double Groups* (Clarendon, Oxford, 1986).

[42] B. Blümich and H. W. Spiess, Quaternions as a practical tool for the evaluation of composite rotations, J. Magn. Reson. **61**, 356 (1985).

[43] C. Councell, C. M. Levitt, and R. R. Ernst, Analytical theory of composite pulses, J. Magn. Reson. **63**, 133 (1985).

[44] M. H. Levitt, Symmetry in the design of NMR multiple-pulse sequences, J. Chem. Phys. **128**, 052205 (2008).

[45] M. Cahay, G. B. Purdy, and D. Morris, On the quaternion representation of the Pauli spinor of an electron, Phys. Scr. **94**, 085205 (2019).

[46] M. Cahay and D. Morris, On the quaternionic form of the Pauli-Schrödinger equation, Phys. Scr. **95**, 015204 (2020).

[47] S. G. Schirmer, A. D. Greentree, V. Ramakrishna, and H. Rabitz, Constructive control of quantum systems using factorization of unitary operators, J. Phys. A **35**, 8315 (2002).

[48] S. Glaser, U. Boscain, T. Calarco *et al.*, Training Schrödinger's cat: quantum optimal control, Eur. Phys. J. D **69**, 279 (2015).

[49] T. Zanon-Willette, M. Minissale, V. I. Yudin, and A. V. Taichenachev, Composite pulses in Hyper-Ramsey spectroscopy for the next generation of atomic clocks, J. Phys.: Conf. Ser. **723**, 012057 (2016).

[50] K. Beloy, Hyper-Ramsey spectroscopy with probe-laser-intensity fluctuations, Phys. Rev. A **97**, 031406(R) (2018).

[51] J. Yepez, *Lecture Notes: Qubit Representations and Rotations*, Phys 711 Topics in Particles and Fields, Spring 2013, Lecture 1 (University of Hawai'i, Manoa, Hawai'i, 2013), Vol. 3.

[52] M. Abramowitz and I. A. Stegun, *Handbook of Mathematical Functions* (Dover, New York, 1968).

[53] S. J. Sangwine and N. Le Bihan, Quaternion polar representation with a complex modulus and complex argument inspired by the Cayley-Dickson form, Adv. Appl. Clifford Alg. **20**, 111 (2010).

[54] R. P. Feynman, Simulating physics with computers, Int. J. Theor. Phys. **21**, 467 (1982).

[55] J.-W. Lee, C. H. Kim, E. K. Lee, J. Kim, and S. Lee, Qubit geometry and conformal mapping, Quant. Inf. Process. **1**, 129 (2002).

[56] A second recursive algorithm related to a Möbius transformation in conformal mapping is based on the following modification with $l \in \{p, q\}(p \to +, q \to -)$ as:

$$\tan\widetilde{\theta}_l \mapsto \frac{\tan\widetilde{\theta}_l + e^{-i\Xi_{l,l+1}}\tan\widetilde{\theta}_{l+1}}{1 - e^{-i\Xi_{l,l+1}}\tan\widetilde{\theta}_l\tan\widetilde{\theta}_{l+1}},$$

where $\Xi_{l,\,l+1} = \phi_l + \phi_{l+1} \pm (\varphi_l - \varphi_{l+1})$.

[57] R. P. Feynman, F. L. Vernon, and R. L. Hellwarth, Geometrical representation of the schrödinger equation for solving Maser Problems, J. Appl. Phys. **28**, 49 (1957).

[58] E. Majorana, Atomi orientati in campo magnetico variabile, Nuovo Cimento **9**, 43 (1932).

[59] F. Bloch and I. I. Rabi, Atoms in variable magnetic fields, Rev. Mod. Phys. **17**, 237 (1945).

[60] J. Schwinger, The Majorana formula, Trans. N. Y. Acad. Sci. **38**, 170 (1977).

[61] T. L. Curtright, D. B. Fairlie, and C. K. Zachos, A compact formula for rotations as spin matrix polynomials, SIGMA **10**, 01 (2014).

[62] R. L. Shoemaker, Coherent transient infrared spectroscopy, in *Laser and Coherence Spectroscopy*, edited by J. I. Steinfeld (Plenum, New York, 1978), pp. 197–371.

[63] R. Valiulin, *NMR Multiplet Interpretation: An Infographic Walk-Through* (De Gruyter, Berlin, Boston, 2019).

[64] F. T. Hioe and J. H. Eberly, N-Level Coherence Vector and Higher Conservation Laws in Quantum Optics and Quantum Mechanics, Phys. Rev. Lett. **47**, 838 (1981).

[65] M. Gell-Mann, Symmetries of baryons and mesons, Phys. Rev. **125**, 1067 (1962).

[66] T. L. Curtright and C. K. Zachos, Elementary results for the fundamental representation of SU(3), Rep. Math. Phys. **76**, 401 (2015).

[67] S. Weigert, Baker-Campbell-Hausdorff relation for special unitary groups SU(N), J. Phys. A **30**, 8739 (1997).

[68] M. Ringbauer, M. Meth, L. Postler, R. Stricker, R. Blatt, P. Schindler, and T. Monz, A universal qudit quantum processor with trapped ions, arXiv:2109.06903.

[69] S. M. Brewer, J.-S. Chen, A. M. Hankin, E. R. Clements, C. W. Chou, D. J. Wineland, D. B. Hume, and D. R. Leibrandt, $^{27}Al^{+}$ Quantum-Logic Clock with a Systematic Uncertainty below 10^{-18}, Phys. Rev. Lett. **123**, 033201 (2019).

[70] J. Ye, H. J. Kimble, and H. Katori, Quantum state engineering and precision metrology using state-insensitive light traps, Science **320**, 1734 (2008).

[71] R. B. Hutson, A. Goban, G. E. Marti, L. Sonderhouse, C. Sanner, and J. Ye, Engineering Quantum States of Matter for Atomic Clocks in Shallow Optical Lattices, Phys. Rev. Lett. **123**, 123401 (2019).

[72] R. Kaubruegger, P. Silvi, C. Kokail, R. van Bijnen, A. M. Rey, J. Ye, A. M. Kaufman, and P. Zoller, Variational Spin-Squeezing Algorithms on Programmable Quantum Sensors, Phys. Rev. Lett. **123**, 260505 (2019).

[73] R. Kaubruegger, D. V. Vasilyev, M. Schulte, K. Hammerer, and P. Zoller, Quantum Variational Optimization of Ramsey Interferometry and Atomic Clocks, Phys. Rev. X **11**, 041045 (2021).

[74] R. Kohlhaas, A. Bertoldi, E. Cantin, A. Aspect, A. Landragin, and P. Bouyer, Phase Locking a Clock Oscillator to a Coherent Atomic Ensemble, Phys. Rev. X **5**, 021011 (2015).

[75] W. Bowden, A. Vianello, I. R. Hill, M. Schioppo, and R. Hobson, Improving the Q Factor of an Optical Atomic Clock Using Quantum Non-Demolition Measurement, Phys. Rev. X **10**, 041052 (2020).

[76] E. Pedrozo-Peñafiel, S. Colombo, C. Shu, A. F. Adiyatullin, Z. Li, E. Mendez, B. Braverman, A. Kawasaki, D. Akamatsu, Y. Xiao, and V. Vuletic, Entanglement-enhanced optical atomic clock, Nature (London) **588**, 414 (2020).

[77] M. Schulte, N. Lörch, I. D. Leroux, P. O. Schmidt, and K. Hammerer, Quantum Algorithmic Readout in Multi-Ion Clocks, Phys. Rev. Lett. **116**, 013002 (2016).

[78] I. Ushijima, M. Takamoto, and H. Katori, Operational Magic Intensity for Sr Optical Lattice Clocks, Phys. Rev. Lett. **121**, 263202 (2018).

[79] M. Braun and S. J. Glaser, Concurrently optimized cooperative pulses in robust quantum control: Application to broadband Ramsey-type pulse sequence elements, New J. Phys. **16**, 115002 (2014).

[80] A. D. Ludlow, M. M. Boyd, J. Ye, E. Peik, and P. O. Schmidt, Optical atomic clocks, Rev. Mod. Phys. **87**, 637 (2015).

[81] Y. Wang, Y. Z. Hu, B. C. Sanders, and S. Kais, Qudits and high-dimensional quantum computing, Front. Phys. **8**, 479 (2020).

[82] C. L. Degen, F. Reinhard, and P. Cappellaro, Quantum sensing, Rev. Mod. Phys. **89**, 035002 (2017).

[83] S. S. Kondov, C.-H. Lee, K. H. Leung, C. Liedl, I. Majewska, R. Moszynski, and T. Zelevinsky, Molecular lattice clock with long vibrational coherence, Nat. Phys. **15**, 1118 (2019).

[84] C. J. Baker, W. Bertsche, A. Capra *et al.*, Laser cooling of antihydrogen atoms, Nature (London) **592**, 35 (2021).